Available online at www.sciencedirect.com
ScienceDirect
Gondwana Research 11 (2007) 553–567
www.elsevier.com/locate/gr

Isotopic evidence on the diagenetic evolution of coastal sabkha reservoirs from the Solimões Basin, northern Brazil

Andreia Dias Elias [a,1], Luiz Fernando De Ros [a,b,*], Ana Maria Mizusaki [a,b], Koji Kawashita [a]

[a] *Instituto de Geociências, Universidade Federal do Rio Grande do Sul, Av. Bento Gonçalves, 9500, 91509-900, Campus do Vale, Porto Alegre (RS), Brazil*
[b] *CNPq, Brazil*

Received 26 January 2006; received in revised form 19 April 2006; accepted 9 June 2006
Available online 3 October 2006

Abstract

The isotopic composition of diagenetic carbonates, sulfates, illites and associated diagenetic constituents of the Carboniferous Juruá sandstones, Solimões Basin, largest hydrocarbon reservoirs of northern Brazil, was analyzed in conjunction with petrographic characterization and chemical composition. Eolian Juruá sandstones, deposited in a coastal sabkha of a wide cratonic sag, are the best reservoirs, but diagenetic processes introduced strong and complex heterogeneities, which affect hydrocarbon production. Dolomite and anhydrite cementation, together with compaction, exerts the main control on the quality of the reservoirs. Early dolomite cements precipitated under strong evaporation, while late dolomites are related to thermal decarboxylation. Late anhydrite cements are related to the interbedded evaporites and possibly to the oxidation of dissolved sulfide. Authigenic illite K–Ar ages are related to the voluminous Triassic basic magmatism (around 200 Ma), and to the Jurassic–Cretaceous tectonism (around 150 Ma), which may have also affected the late anhydrite and dolomite–ankerite cementation. This isotopic study revealed the major conditions of the diagenetic processes that strongly affected the Juruá reservoirs, which are essential for the development of models that will optimize the production, as well as decrease the risks in the exploration for new Juruá reservoirs.

Keywords: Sandstone diagenesis; Coastal sabkha; Isotopes; Dating; Reservoir quality

1. Introduction

The diagenetic evolution of the Carboniferous sandstones of the Juruá Formation, Solimões Basin, northern Brazil, is highly complex, and promoted the introduction of strong heterogeneity in these largest hydrocarbon reservoirs of northern Brazil. The objective of this study is to use the isotopic characteristics of diagenetic constituents of the Juruá sandstones, particularly of the carbonates, sulfates and illites, supported by the petrographic characterization and chemical composition of these and associated constituents, in order to define the paragenetic evolution of the reservoir sandstones and to understand the genetic conditions and distribution of the diagenetic processes. This understanding is important for the development of geochemical models that will improve the efficiency of development and production of the reservoirs, as well as to decrease the risks of exploration for Juruá reservoirs in the basin.

2. Geological setting

The study area is situated in the Solimões Basin. This is a large Paleozoic basin, covering around 600,000 km^2 of the Amazonian Craton (northern Brazil). The Basin is limited to the south by the Brazilian Shield, to the north by the Guyanas Shield, to the west by the Acre Basin across the Iquitos Arch, and to the east by the Amazonas Basin across the Purus Arch (Caputo and Silva, 1990; Eiras et al., 1994; Fig. 1).

The Carauari Arch divides the Solimões Basin into the Jandiatuba and the Juruá sub-basins, having exerted an

* Corresponding author. Instituto de Geociências, Universidade Federal do Rio Grande do Sul, Av. Bento Gonçalves, 9500, 91509-900, Campus do Vale, Porto Alegre (RS), Brazil. Fax: +55 51 3316 7302.
E-mail addresses: andreia.elias@petrobras.com.br (A.D. Elias), lfderos@inf.ufrgs.br (L.F. De Ros).
[1] Present address: PETROBRAS UN-RIO/ST/CER, Av. General Canabarro, 500, Rio de Janeiro, Brazil.

1342-937X/$ - see front matter © 2006 International Association for Gondwana Research. Published by Elsevier B.V. All rights reserved.
doi:10.1016/j.gr.2006.06.007

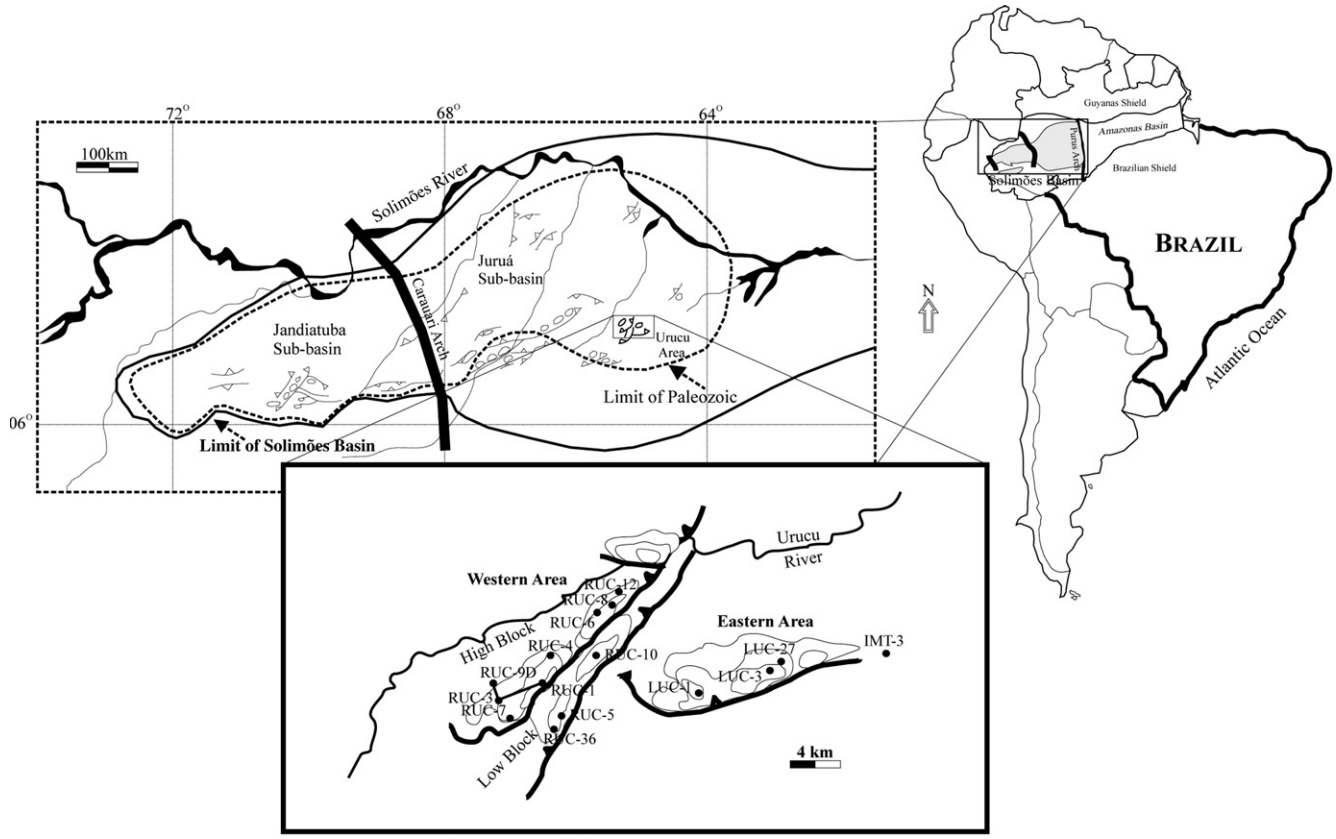

Fig. 1. Location map of the studied area, showing the position of structural section of Fig. 8 (modified from Elias et al., 2004).

important control over the pre-Pennsylvanian sedimentation (Neto and Tsubone, 1988; Eiras et al., 1994).

The Solimões Basin was originated as an intracratonic sag and filled by six depositional sequences, known as the Ordovician, Silurian–Devonian, Devonian–Carboniferous, Carboniferous–Permian, Cretaceous and Tertiary sequences (Eiras et al., 1994). The basal part of the Carboniferous–Permian sequence, known as the Juruá Formation, is the main target of this study (Fig. 1).

An extensive Late Triassic to Early Jurassic basic magmatism (Mizusaki et al., 2002), represented by large diabase intrusions, is interpreted to have influenced the generation, expulsion, migration and accumulation of hydrocarbons in the basin (Figueiredo and Milani, 2000).

The Juruá Formation is the most important hydrocarbon reservoir of the Solimões Basin containing over 190×10^9 m^3 of gas in place and 110×10^6 m^3 of associated oil (ANP home page). The accumulations of the Juruá Formation are aligned along the Solimões mega-shear zone, related to a fault-and-fold system with N70°–80°E direction caused by a Jurassic to Cretaceous right-lateral wrenching (Caputo and Silva, 1990). The sedimentary-tectonic evolution in the studied area starts with an extensional event characterized by normal faults and source area uplift related to the Eohercinian tectonism, followed by the Jurassic–Cretaceous transpressional tectonism, which originated reverse faults and folds, and gave the area its present configuration (Camoleze et al., 1990).

3. Depositional environment

The Juruá Formation is constituted by sandstones, mudrocks (mudstones), evaporites and dolostones deposited in a fluvial–deltaic environment with pervasive eolian reworking. Towards its top, the unity grades to a coastal eolian environment under increasing marine influence, culminating with beach facies, eolian reworking and longitudinal bars and tidal deltas (cf. Becker, 1997; Milani and Zalán, 1998). The climate was hot and arid as indicated by the association of sabkha evaporites and dunes (Lanzarini, 1984; Cunha et al., 1988; Becker, 1997; Milani and Zalán, 1998). The eolian sandstones are considered the best reservoirs of the Juruá Formation. The description of cores from 13 boreholes indicates that the deposition of the studied reservoirs occurred in a coastal sabkha system with important eolian contribution (Elias et al., 2004).

The portion of the Juruá Formation analyzed in this study contains the major reservoirs and is divided into five operational units, from base to top: JR-90A, JR-85, JR-80, JR 70A and 70B. The stratigraphy of the studied area is characterized by four stacked drying and drying–wetting-upward cycles, similar to what is recognized in the Rotliegend reservoirs (Amthor and Okkerman, 1998). These cycles are constituted by sabkha facies in the base overlain by eolian sand sheet and dune deposits, which are in turn overlain again by sabkha deposits. The wetting-upward portion of each cycle

is commonly eroded by the next cycle, being preserved only in some cores.

4. Sampling and methods

In this study, 300 epoxy-impregnated thin-sections sampled from cores of 13 wells comprising of depths of 2420–2585 m were examined with standard petrographic microscopes. The volumes of detrital, diagenetic components, and pore types were determined by counting 300 points in 122 representative thin-sections.

Twenty-six thin-sections were carbon-coated and analyzed with a Cameca Camebax SX50 electron microprobe (EMP) equipped with four spectrometers and a backscattered electron detector (BSE). The operating conditions were an acceleration voltage of 15 kV and a beam current of 8 nA and 5 μm of diameter for carbonates and 10 nA and 1 μm for feldspars.

The habits and paragenetic relationships of diagenetic minerals were examined in nine gold-coated sandstone chip samples with a JEOL JSM-5800 scanning electron microscope (SEM) with an acceleration voltage of 20 kV, a beam current of 69 nA, and a coupled energy-dispersive (EDS) probe.

Thirty sandstone samples were selected for O and C isotopes analyses in the dolomite and siderite cements after sequential chemical separation treatments (Al-Aasm et al., 1990). The dolomites were reacted at 25 °C for 72 h after removal of traces of calcite, and the siderites were reacted at 50 °C for 72 h after dolomite removal. The evolved gas for each carbonate fraction was analyzed using a SIRA-12 mass spectrometer. The phosphoric acid factors were 1.01060 for dolomite and 1.010454 for siderite (Rosenbaum and Sheppard, 1986). Precision (1σ) was monitored through daily analysis of the NBS-20 calcite standard and was better than ±0.05‰ for both $\delta^{13}C$ and $\delta^{18}O$. Carbon isotope data are presented in the normal δ notation relative to V_{PDB} standard (Craig, 1957) and oxygen isotope in the V_{PDB} and V_{SMOW} patterns.

Twenty-four samples (22 sandstones and two evaporites) were selected for O and S isotopes analyses of the anhydrites. The O isotopes were analyzed with a MAT252 spectrometer after $BaSO_4$ conversion of the sulfates and conventional BrF_5 extraction. The S isotopes were analyzed using CF-IRMS. Sulfur isotope data are presented in the normal δ notation relative to CDT standard (Thode et al., 1961). Accuracy was within ±0.2‰.

Fifteen samples from dolomite and anhydrite cements were analyzed for the $^{87}Sr/^{86}Sr$ ratio recognition. The phases separation follows a procedure modified from Schultz et al. (1989) and Dworkin and Land (1994). The isotopic ratios were obtained from the analysis of the sample preparation in cation exchange columns by a VG-Sector 54 mass spectrometer. The samples were standardized by $^{86}Sr/^{88}Sr$ at 0.1194, assuming a fraction of $^{87}Sr/^{86}SrN$ of 0.71025 based on $SrCO_3$ NBS-987 standard.

Fine fraction (FF) separation for K–Ar dating of the authigenic illites required successive processes of ultrasound disaggregation and centrifuge concentration (Mizusaki et al., 1990). Around 0.5 g of the $0.1<FF<0.5$ μm fraction was separated from each of the selected samples of approximately 1 kg. The purity of the illite concentrate was controlled by X-ray diffraction analyses. The $^{40}K–^{40}Ar$ dating of the illite fractions was performed in a nuclide mass spectrometer of Reynolds type, following, with small adaptations, the recommendations of Amaral et al. (1966) and the calculation constants proposed by Steiger and Jager (1977).

In this paper, the terms *eo-*, *meso-* and *telodiagenesis* are applied for the diagenetic stages *sensu* Schmidt and McDonald (1979). *Eodiagenesis* include processes under the direct influence of depositional fluids at relatively shallow depths and relatively low temperatures (typically <70 °C), whereas *mesodiagenesis* includes the reactions involving chemically evolved formation of waters under effective burial and higher temperatures. *Telodiagenesis* refers to those processes related to the uplift and exposure of sandstones to near-surface meteoric conditions, or due to the penetration of meteoric fluids along basin margins and major faults, after burial and mesodiagenesis.

5. Detrital composition

The Juruá sandstones are mostly subarkoses and arkoses (*sensu* Folk, 1968; Fig. 2). The quartz grains are essentially monocrystalline plutonic, comprising in average volume of 51% bulk sandstone and reaching up to 58.7% in the eolian sandstones and 68.3% in the non-eolian sandstones. Polycrystalline quartz grains are less common, making in average 5.4% of the eolian and 4% of the non-eolian sandstones. Detrital feldspars are dominantly microcline (average of 4%), being orthoclase, perthite and plagioclase subordinated. The K-feldspars show limited dissolution processes and replacement by illite and albite. The plagioclases are also partially albitized and illitized. The rock fragments include plutonic, volcanic, sedimentary and metamorphic types, the granitic–gneissic plutonic fragments being the most abundant. Accessory detrital constituents include heavy minerals, micas, mud intraclasts, dolomite intraclasts and clay peloids. The mud intraclasts commonly show dissolution, compaction into

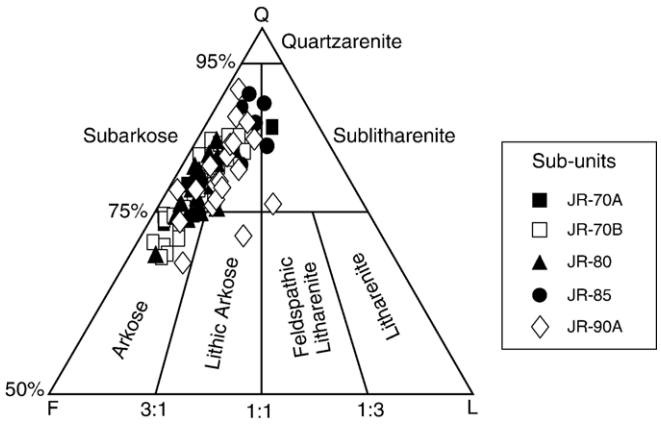

Fig. 2. Present and original detrital composition of the sandstones from the studied sub-units of Juruá Formation, plotted on the upper half of Folk (1968) diagram.

pseudomatrix and illitization. The clay peloids are usually covered by microcrystalline dolomite rims.

6. Diagenetic minerals

6.1. Dolomite and ankerite

Dolomite is the most abundant diagenetic constituent in the Juruá reservoir (7.5% average of up to 68%) which occurrs in every depositional facies and sub-unit. It occurs mostly as microcrystalline (10–50 μm) pore-filling cement. In this habit, dolomite comprises in average of 3.1% bulk volume (up to 16%) and is more common in the eolian sandstones (average of 3.9%). Pore-filling microcrystalline dolomite contains 0.8–4% $FeCO_3$. Microcrystalline dolomite also occurs as rims (Fig. 3A average of 0.3% up to 11%), which contain 0.8–7.3% $FeCO_3$. Such dolomite rims average 0.4% (up to 11%) in the eolian sandstones and 0.2% (up to 2%) in the non-eolian sandstones. The carbon and oxygen isotope values of microcrystalline dolomites range between −6.36‰ and +0.69‰ $\delta^{13}C_{V\text{-}PDB}$ and between −6.85‰ and −1.48‰ $\delta^{18}O_{V\text{-}PDB}$ (Table 1). The $^{87}Sr/^{86}Sr$ ratio values range between 0.7097048 and 0.7123545 (Fig. 4 and Table 2).

Dolomite also occurs as 0.1–0.5 mm wide blocky (euhedral) crystals (Fig. 3B) which average at 1.6% (up to 26%). Blocky dolomite averages 0.8% (up to 19%) in eolian sandstones, mostly in JR-70A and JR-90A sub-units, but it is more abundant in the non-eolian sandstones, averaging 2.4% (up to 18% in the JR-70A). The compositional zonation of blocky dolomite ranges between 5.4% and 25% of $FeCO_3$ (ankerite). Ankerite usually occurs as irregular overgrowths on dolomite crystals (Fig. 3C). The C and O isotope values of this dolomite type vary between −8.89‰ and +1.93‰ $\delta^{13}C_{V\text{-}PDB}$ and between −12.19‰ and −1.81‰ $\delta^{18}O_{V\text{-}PDB}$

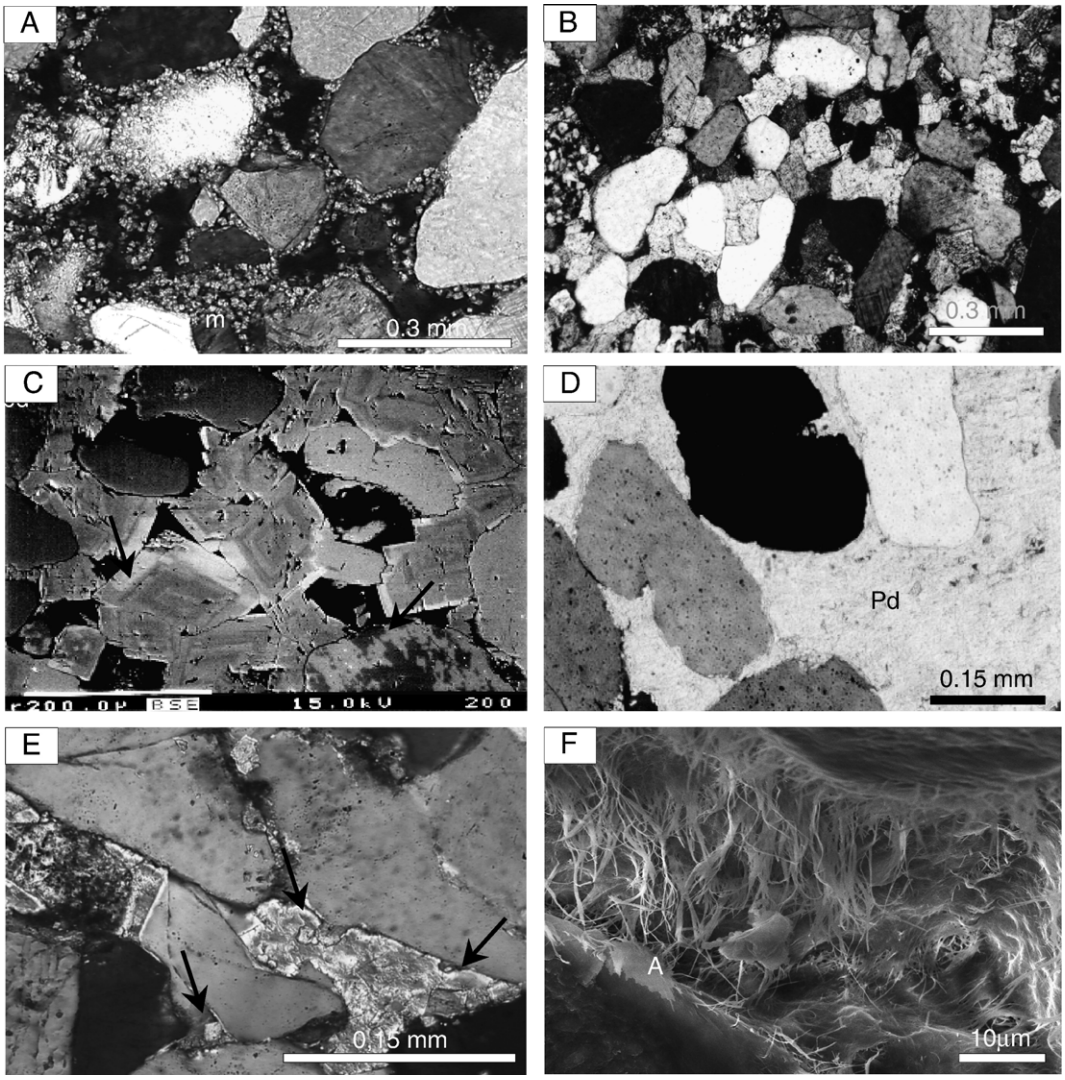

Fig. 3. (A) Optical photomicrograph of a sandstone cemented by microcrystalline dolomite rims; crossed polarizers (XP). (B) Optical photomicrograph of a sandstone cemented by blocky pre-compactional dolomite (XP). (C) Backscattered electrons (BSE) image of zoned blocky dolomite cement with ankerite overgrowths (arrows). (D) Optical photomicrograph of poikilotopic anhydrite cement engulfing dolomite crystals (arrows) (XP); (E) optical photomicrograph of poikilotopic, replacive dolomite cement (Pd) (XP). (F) Scanning electron (SEM) image of fibrous illite forming bridges between grains.

Table 1
Isotopic values and calculated precipitation temperatures of dolomites and siderites from the Juruá Formation

Well	Depth (m)	$\delta^{13}C$ (VPDB)	$\delta^{18}O$ (VPDB)	$\delta^{18}O$ (SMOW)	Carbonate	Timing	$\delta^{18}O$ water	*T* precip. °C
LUC-1	2448.20	−4.30	−1.48	29.34	Fine dolomite rims	Pre-compaction	−1	34.6
IMT-3	2459.81	−1.56	−1.57	29.24	Dolocrete	Pre-compaction	−1	35.1
RUC-5	2519.80	−0.60	−1.81	28.99	Blocky dolomite	Pre-compaction	−1	36.5
IMT-3	2477.52	0.12	−1.82	28.98	Blocky displacive dolomite	Pre-compaction	−1	36.6
RUC-1	2440.30	1.93	−2.81	27.96	Blocky dolomite	Pre-compaction	−1	42.5
RUC-12	2508.50	0.70	−2.82	27.95	Blocky dolomite	Pre-compaction	−1	42.6
LUC-1	2426.70	1.28	−3.21	27.55	Blocky dolomite	Pre-compaction	−1	45.0
RUC-10	2505.70	1.49	−3.72	27.03	Blocky dolomite	Pre-compaction	−1	48.3
LUC-1	2452.40	−6.36	−3.77	26.97	Fine displacive dolomite	Pre-compaction	−1	48.6
LUC-27	2472.79	−1.36	−4.18	26.55	Fine dolomite	Pre-compaction	−1	51.3
LUC-3	2442.30	−0.62	−4.20	26.53	Fine dolomite	Pre-compaction	−1	51.4
IMT-3	2460.95	0.69	−4.34	26.33	Fine dolomite rims	Pre-compaction	−1	52.3
RUC-1	2442.90	1.14	−4.36	25.92	Fine and blocky dolomite	Pre-compaction	−1	52.5
RUC-10	2520.50	−0.29	−4.69	26.03	Fine dolomite	Pre-compaction	−1	54.7
RUC-7	2502.96	0.43	−4.87	25.84	Fine dolomite	Pre-compaction	−1	55.9
LUC-27	2485.57	−5.06	−5.14	25.56	Fine displacive dolomite	Pre-compaction	−1	57.8
IMT-3	2473.42	−4.00	−5.39	25.30	Fine and Blocky dolomite	Pre-compaction	−1	59.5
RUC-36	2514.55	−1.81	−5.70	24.98	Fine dolomite	Pre-compaction	−1	61.7
LUC-27	2460.13	−3.71	−5.89	24.79	Fine dolomite	Pre-compaction	−1	63.1
RUC-5	2508.85	−2.68	−6.26	24.40	Fine dolomite rims	Pre-compaction	−1	65.8
RUC-36	2517.55	−2.94	−6.85	23.80	Fine dolomite	Pre-compaction	−1	70.2
RUC−1	2548.60	−5.11	-6.43	24.23	Poikilotopic dolomite	Post−compaction	3	99.4
RUC-1	2550.20	−5.04	−6.63	24.03	Poikilotopic dolomite	Post-compaction	3	101.1
LUC-3	2456.90	−5.13	−7.76	22.86	Poikilotopic dolomite	Post-compaction	3	111.3
LUC-3	2461.40	−4.61	−7.92	22.60	Poikilotopic dolomite	Post-compaction	3	112.8
RUC-7	2509.50	−6.76	−8.48	22.12	Blocky replacive dolomite	Post-compaction	3	118.0
RUC-7	2521.51	−8.45	−10.72	19.39	Poikilotopic dolomite	Post-compaction	3	140.0
LUC-1	2454.70	−8.89	−12.19	18.29	Blocky replacive dolomite	Post-compaction	3	155.4
LUC-3	2461.40	−4.64	−7.48	23.16	Poikilotopic Siderite	Post-compaction	3	72.0
LUC-3	2456.90	−5.20	−7.51	23.19	Poikilotopic Siderite	Post-compaction	3	72.0
RUC-7	2521.51	−7.20	−9.00	21.53	Poikilotopic Siderite	Post-compaction	3	82.0

(Table 1). The value of $^{87}Sr/^{86}Sr$ ratio is around 0.7146637 (Fig. 4 and Table 2). The microcrystalline and blocky dolomites are commonly covered and engulfed by poikilotopic anhydrite and by quartz overgrowths.

In places, dolocretes with up to 67% of displacive blocky and microcrystalline dolomite and floating grains occur, mostly interbedded with the non-eolian sandstones of JR-70A and JR-80 sub-units. The isotopic analysis of a representative sample of dolocrete yielded values of −1.56‰ $\delta^{13}C_{V\text{-}PDB}$ and −1.57‰ $\delta^{18}O_{V\text{-}PDB}$.

Another habit of dolomite is poikilotopic (Fig. 3D), which generally has a heterogeneous distribution in the sandstones, averaging 0.1% (up to 3%), and contains 4–5% of $FeCO_3$. It commonly replaces detrital grains marginally and quartz overgrowths. Isotopic carbon and oxygen analyses in poikilotopic dolomites yielded values between −8.45‰ and −4.61‰ $\delta^{13}C_{V\text{-}PDB}$ and between −10.72‰ and −6.43‰ $\delta^{18}O_{V\text{-}PDB}$ (Table 1). The $^{87}Sr/^{86}Sr$ ratio values range between 0.717 and 0.7219222 (Fig. 4 and Table 2).

6.2. Calcite and siderite

Calcite and siderite are rare in the Juruá sandstones, being restricted to the JR-85 and JR-90A sub-units. Poikilotopic calcite occurs locally (RUC-7 and LUC-3), averaging less than 0.1% (up to 4%), and contains 1–4% $FeCO_3$. Siderite occurs in

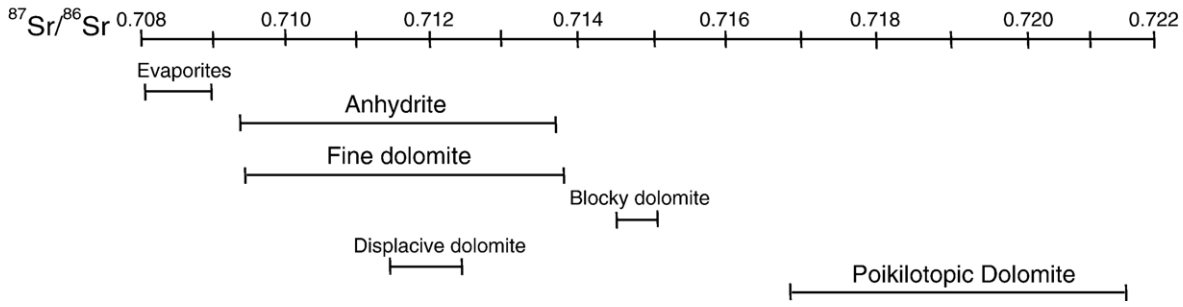

Fig. 4. Distribution of the $^{87}Sr/^{86}Sr$ ratios from the analyzed samples (see Table 2).

Table 2
$^{87}Sr/^{86}Sr$ ratios for dolomites and anhydrites of the Juruá Formation

Well	Depth (m)	Sample	$^{87}Sr/^{86}Sr$
RUC-10	2516.5	Fine dolomite	0.7123545
RUC-1	2440.3	Fine dolomite	0.7117691
LUC-27	2464.6	Fine dolomite	0.7098969
RUC-12	2521.4	Fine dolomite	0.7098641
IMT-3	2460.9	Fine dolomite	0.7097048
LUC-1	2426.7	Displacive dolomite	0.7117738
LUC-1	2454.9	Blocky dolomite	0.7146637
RUC-1	2550.2	Poikilotopic dolomite	0.7219222
LUC-3	2455.6	Poikilotopic dolomite	0.7170539
RUC-5	2535.4	Evaporite	0.7089167
RUC-5	2512.5	Anhydrite	0.7132570
RUC-5	2550.9	Anhydrite	0.7132060
LUC-1	2448.2	Anhydrite	0.7096907
LUC-27	2478.2	Anhydrite	0.7137169

places (LUC-3, average of 0.1% up to 2%), with a poikilotopic habit, associated to calcite and dolomite, and contains 9–10% $MgCO_3$. Isotope analysis of these siderites yielded values between −7.2‰ and −4.64‰ $\delta^{13}C_{V\text{-}PDB}$ and from −9‰ to −7.48‰ $\delta^{18}O_{V\text{-}PDB}$ (Table 1).

6.3. Anhydrite

Anhydrite is the second most important diagenetic constituent in Juruá sandstones, and occurs in every sub-unit, facies and area, making in average 5% of the bulk volume (up to 26.3%). The distribution of anhydrite and dolomite shows a negative covariance, with larger amounts of anhydrite in sandstones with less microcrystalline or blocky dolomite. Anhydrite occurs most commonly as pore-filling, poikilotopic cement, and rarely lamellar. Distribution is heterogeneous, as scattered spots, or selectively cementing the coarser laminations. Anhydrite covers the quartz overgrowths and engulfs the dolomite (Fig. 3E). Anhydrite dissolution is limited (average of 0.1% up to 1.7%). In places, some silicification of the anhydrite to chalcedony or microquartz is observed. Anhydrite replaces quartz and feldspar grains, as well as dolomite crystals and pseudomatrix. Isotope analysis of anhydrite yielded values between 9.5‰ and 17.8‰ $\delta^{34}S_{CDT}$ and from −1.2‰ to −19.75‰ $\delta^{18}O_{V\text{-}PDB}$ (Table 4). The $^{87}Sr/^{86}Sr$ values of the anhydrite cements range from 0.7096907 to 0.7137169, while a nodular evaporitic anhydrite layer yielded a value of 0.7089167 (Table 2).

6.4. Quartz and K-feldspar overgrowths

Quartz overgrowths are also an important diagenetic constituent in the Juruá sandstones (average of 2% up to 21%). Quartz overgrowth cementation is very common in the non-eolian sandstones of JR-80, JR-85 and JR-90A sub-units as well as in the eolian sandstones of JR-90A sub-unit. Quartz cement rarely occurs as prismatic outgrowths. The overgrowths commonly cover clay mineral coatings, engulf dolomite crystals, and are covered by anhydrite and illite (Fig. 3E). The extremely small size of fluid inclusions within quartz overgrowths (<20 μm) has rendered impossible to obtain information on the temperature and salinity of precipitating fluids.

The occurrence of sutured intergranular contacts and stylolites in sandstones devoid of abundant dolomite or anhydrite cements suggests that at least part of the Si for quartz overgrowth precipitation was internally derived. However, as the distribution of intergranular chemical compaction and stylolites is extremely heterogeneous, it is not possible to be precise if internal pressure dissolution is sufficient to explain the observed amounts of quartz cement.

K-feldspar overgrowths are substantially less common and much less abundant than quartz overgrowths (average of 0.1% up to 0.7%, mostly in non-eolian sandstones of JR-80 and JR-90A sub-units), being more common on microcline than on orthoclase grains.

6.5. Diagenetic clay minerals

Thin clay mineral coatings cover discontinuously the detrital grains in every sub-unit (average of 0.4% up to 4%). Non-eolian sandstones show thicker coatings, with irregular shape indicative of mechanical clay infiltration. X-ray diffraction analyses have shown that the coatings are constituted of regular illite–smectite, probably evolved from detrital infiltrated smectites (Moraes and De Ros, 1992). Clay coatings are conspicuous along sutured intergranular and stylolitic pressure dissolution contacts.

The small volume and thickness of the mechanically infiltrated clay coatings indicates a very limited meteoric water supply, probably due to the severe aridity of the environment and to the absence of alluvial systems fed by influent episodic floods. The small thickness of the coatings prevented any influence of these clays on the following cementation by quartz, dolomite or anhydrite. During subsequent burial, the originally smectitic infiltrated clays (Moraes and De Ros, 1990) were transformed into illite–smectite honeycombed aggregates later covered by fibrous illite.

Authigenic illite occurs mostly as fibrous aggregates, which partially fill intergranular and intragranular pores (within dissolved feldspars) and form bridges between grains (Fig. 3F), but also replaces volcanic rock fragments and feldspar grains. Illite averages only trace % in the unit, being more common (average of 0.4% up to 2.3%) in the non-eolian sandstones than in the eolian sandstones (average of 0.1% up to 1%).

The values obtained with ^{40}K–^{40}Ar dating applied in illites concentrated in fraction $0.1 < FF < 0.5$ μm indicate a medium absolute age around 200 Ma (Table 3) to the illites of the reservoirs JR-60, JR-70B and JR-90B. Otherwise, the dating of illites of reservoir R7A yielded an age of 150 Ma, characterizing two important stages concerning the precipitation of authigenic illites in the Juruá sandstones of the area.

Chlorite occurs in trace amounts in the eastern area, associated to illite and mixed layers I/S as rims of lamellae with lobate edges. Kaolinite is very rare, and observed only in trace amounts as intergranular aggregates.

Table 3
$^{40}K/^{40}Ar$ ages of diagenetic illites (0.1<FF<0.5 mm fraction; modif. Mizusaki et al., 1990)

Reservoir	K/Ar ages (Ma)	Hydrocarbon
JR-60	199.3±24.9	Gas
JR-70A	153.1±1.8	Gas
JR-70B	209.9±2.6	Gas
JR-90B	202.2±3.5	Oil

6.6. Other diagenetic minerals

Albite partially replaces K-feldspar and plagioclase grains, with the chemically pure $NaAlSi_3O_8$ composition typical of diagenetic albite as parallel aggregates of prismatic crystals. Framboidal pyrite aggregates fill pores and replace grains, and are engulfed by other cements. The occurrence of hematite coatings is much less common in Juruá sandstones than in other sandstones with similar depositional environment (Pye and Krinsley, 1986; Dixon et al., 1989; Purvis, 1992), being restricted only to some water zone samples in JR-90A sub-unit in the extreme eastern area (IMT). This can be related to the dissolution of iron oxides during burial by strongly reducing fluids associated to hydrocarbon migration. The oxidation along the margins of poikilotopic dolomite and siderite crystals, locally associated to pore-filling kaolinite, is interpreted as a product of telodiagenesis, which potentially occurred during Mesozoic uplift (Jurassic–Cretaceous tectonism). Anatase occurs as scattered crystals filling pores and replaces detrital heavy mineral grains. Poikilotopic barite was observed only in trace amounts associated to poikilotopic siderite and dolomite. Halite occurs in trace amounts in the JR-90A sub-unit, associated to fibrous illite.

7. Discussion

7.1. Conditions of dolomite precipitation

The precipitation of dolomite in the Juruá sandstones started soon after deposition and close to surface. This can be inferred by the loose packing of the sandstones massively cemented by microcrystalline dolomite and of some cemented by coarse blocky dolomite, as well as by the occurrence of dolocretes with cement-supported fabric.

The common occurrence of microcrystalline dolomite in the eolian sandstones suggests precipitation from highly concentrated pore fluids due to evaporation within the eolian deposits during early diagenesis. The dominance of microcrystalline dolomite under these conditions is probably related to the decrease in the Ca^{2+}/Mg^{2+} ratio due to the precipitation of evaporitic sulfates, but in some cases could also be related to the mixture of marine and meteoric waters (Morad et al., 1992). Pre-compactional dolomite cements are characterized by lower Fe content relative to post-compactional cements. This may be related both with the dominantly referred to oxidizing conditions during the early diagenesis of the unit and to an increasing contribution of Fe from interbedded mudrocks during burial.

On the other hand, the distribution of blocky dolomite cements and of dolocretes in the non-eolian sandstones indicates a larger supply of dissolved HCO_3^-, Mg^{2+} and Ca^{2+} in the transitional sabkha areas. The abundance of eogenetic dolomite in the Juruá sandstones is similar to what is observed in other units deposited in eolian environments associated with coastal sabkhas (Mankiewicz and Steidtmann, 1979; Pye and Krinsley, 1986; James, 1992; Morad et al., 1995).

The wide range of $\delta^{18}O_{V\text{-}SMOW}$ values of dolomite cements (Table 1) indicates the precipitation that took place from fluids varying from marine to possibly meteoric and diagenetic burial, in a wide temperature range, such as observed in the dolomite cements in the Rotliegende reservoirs (Amthor and Okkerman, 1998). The recrystallization of pre-compaction dolomite cements during mesodiagenesis could be invoked to explain the most negative $\delta^{18}O_{V\text{-}SMOW}$ values (as low as −6.85‰ for microcrystalline dolomite). However, there is no petrographic evidence of any recrystallization of eodiagenetic dolomite cements during burial.

The oxygen isotope values of microcrystalline dolomites are presented at Table 1. Assuming a value of −1‰ $\delta^{18}O_{V\text{-}SMOW}$ for the precipitating fluids, which would correspond to the mixture of non-glacial marine and low-latitude meteoric waters expected for a tropical coastal sabkha, a precipitation temperature range of 34.6–70.2 °C is calculated (Table 1). Such temperature interval is consistent with the loose packing of the cemented sandstones, which indicates cementation under near-surface to shallow-burial depths. A purely marine $\delta^{18}O_{V\text{-}SMOW}$ value of −1.2‰ would correspond to an unrealistic temperature range of 48–87.6 °C, which is considered too high for the precipitation of these pre-compactional cements.

Similar conditions are interpreted for the pre-compactional blocky dolomite cements, corresponding to precipitation temperatures of 36.5–48.3 °C, calculated assuming the same $\delta^{18}O_{V\text{-}SMOW}$ value of −1‰ for the precipitating fluids. Likewise, the isotopic values of a representative sample of dolocrete would suggest a near-surface precipitation temperature of 35.1 °C (Table 1).

Such temperature range would correspond to the maximum diurnal variation for the temperatures in sediments at the surface of desertic–evaporitic tropical environments (Parton, 1984; Kemp et al., 1992; both *apud* Amthor and Okkerman, 1998).

Some of the carbon isotopes values of microcrystalline dolomites and of the pre-compactional blocky dolomites are within the range expected for derivation from marine Carboniferous cements (Veizer, 1992). Many of the values of the microcrystalline dolomites are, however, depleted in ^{13}C in relation to the marine range (as low as −6.36‰ $\delta^{13}C_{V\text{-}PDB}$). Such low values of $\delta^{13}C_{V\text{-}PDB}$, combined with the relatively high values of $\delta^{18}O_{V\text{-}SMOW}$ of these cements (Table 1), are probably related to the mixture of dissolved carbonate from marine waters with CO_2 generated by bacterial sulfate reduction. This is compatible to the presence of framboidal pyrite aggregates in some of these samples. On the other hand, the scarcity of framboidal pyrite in most of the sandstones in an environment rich in dissolved sulfate, as suggested by the recurrent interbedding of evaporites, indicates that oxidizing

conditions prevailed during most of the early diagenesis of the sandstones.

The isotopic values of poikilotopic dolomites and of post-compactional, grain replacive blocky dolomites (Table 1) are indicative of higher precipitation temperatures during burial, which agrees with the tighter packing and smaller intergranular volume of these samples. Some of these late dolomite cements are rich in iron (as much as 25% $FeCO_3$), which is common in mesodiagenetic dolomite cements in many units (Boles, 1978; Pye and Krinsley, 1986; Sullivan et al., 1990; Souza et al., 1995; Anjos et al., 2000; Hendry et al., 2000).

We assumed a $\delta^{18}O_{V\text{-}SMOW}$ value +3‰ for the burial diagenetic fluids responsible for the precipitation of post-compactional dolomite, which is typical for formation of waters evolved through substantial rock–fluid interaction during burial diagenesis (Land and Fisher, 1987; Morad et al., 2003). Based on this assumption and using the fractionation equation of Fisher and Land (1986), the precipitation temperature of the post-compactional dolomite cements is calculated at 99–155 °C (Table 1).

The carbon isotopic values of poikilotopic dolomites and of post-compactional, grain-replacive blocky dolomites (Table 1) are compatible with the derivation of these cements from the thermal decarboxylation of organic matter during burial. The positive co-variance of $\delta^{13}C_{V\text{-}PDB}$ and $\delta^{18}O_{V\text{-}PDB}$ values (Fig. 5) suggests an increasing input from thermal decarboxylation over the early diagenetic dominantly marine carbonate source during progressive burial, such as observed in other clastic units (Macaulay et al., 1998).

The $^{87}Sr/^{86}Sr$ ratio for the microcrystalline dolomites ranges from 0.7097048 to 0.7123545 (Table 2). These are relatively low values, yet higher than those expected for cements directly derived from Carboniferous sea waters with $^{87}Sr/^{86}Sr$ around 0.708±0.00025 (Burke et al., 1982; Fig. 6). Such elevated

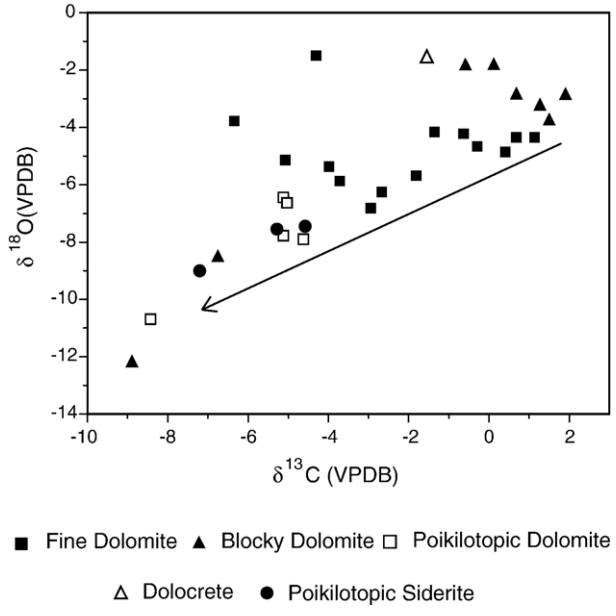

Fig. 5. Diagram of the $\delta^{18}O_{V\text{-}PDB}$ and $\delta^{13}C_{V\text{-}PDB}$ values of dolomite cements from Juruá reservoirs.

$^{87}Sr/^{86}Sr$ values are consistent with the interaction between detrital silicates and meteoric waters in a continental setting.

The pre-compactional blocky dolomite show higher $^{87}Sr/^{86}Sr$ values, around 0.7146637, and is also probably influenced by meteoric waters, as is suggested by the hematite inclusions within some of these crystals.

Therefore, the strontium isotopic values of the dolomite precipitating fluids are quite wide and higher than those proposed for marine waters (Fig. 6). These values can be related to the input of radiogenic ^{87}Sr, which may have been derived from the leaching of acidic basement magmatic rocks with high original $^{87}Sr/^{86}Sr$ ratios. Similar conclusions were drafted by Platt (1994) for the $^{87}Sr/^{86}Sr$ ratios (0.70935–0.71387) of dolomites from the Rotliegende sandstones of northern Germany.

The analyses of the poikilotopic dolomites yielded even higher values for the $^{87}Sr/^{86}Sr$ ratios (0.7171–0.721; Table 2), indicating extensive contribution of radiogenic ^{87}Sr. This ^{87}Sr probably derived from the dissolution of feldspars and other silicates during burial.

7.2. Siderite cementation

Siderite is a mineral adequate for the study of the isotopic evolution of pore waters, as it is normally not affected by recrystallization or isotopic re-equilibration, and has no polymorphs (Gauthier, 1982). The narrow range of $\delta^{18}O_{V\text{-}PDB}$ values of the poikilotopic siderite cements (Table 1) indicates a limited temperature precipitation interval for these phases. Assuming the same +3‰ $\delta^{18}O_{V\text{-}SMOW}$ value for the burial diagenetic fluids responsible for the precipitation of post-compactional dolomite typical for formation of waters evolved through substantial rock–fluid interaction during burial diagenesis (Land and Fisher, 1987; Morad et al., 2003), and using the fractionation equation of Carothers et al. (1988), the precipitation temperature of the poikilotopic, post-compactional siderite cements is calculated at 72–82 °C (Table 1), within the range of burial dolomite cements.

The $\delta^{13}C_{V\text{-}PDB}$ values of the poikilotopic siderite cements (Table 1) have values compatible to a contribution from thermal decarboxylation of organic mater. Also their co-variance with the $\delta^{18}O_{V\text{-}PDB}$ values are well within the trend of the dolomite cements that indicates progressive contribution from the thermal decarboxylation over the early diagenetic marine carbonate source during progressive burial.

7.3. Anhydrite cementation

The abundant precipitation of anhydrite cement is certainly related to the number and thickness of evaporite beds covering and interbedded with the Juruá sandstones. Anhydrite cementation is also more abundant close to the stratigraphic sequence boundaries, which suggests a precipitation controlled by the enhanced fluid circulation along the coarser, more permeable sequence-basal sands during burial. In this case, the source of the mesodiagenetic anhydrite cements could be either the sulfate beds intercalated in the Juruá Formation, or the

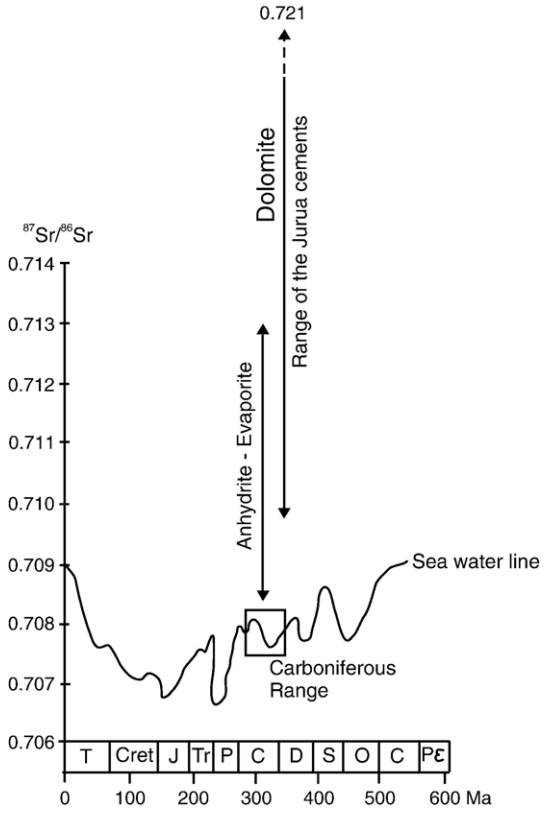

Fig. 6. Variations of the marine $^{87}Sr/^{86}Sr$ ratios with age compared to the values of $^{87}Sr/^{86}Sr$ in dolomite and anhydrite cements of Juruá sandstones (modified from Burke et al., 1982).

overlaying marine evaporite deposits of the Carauari Formation (Becker, 1997). The extensive faulting promoted by the Jurassic–Cretaceous tectonism could have provided pathways for enhanced flow of fluids during mesodiagenesis. A similar derivation of mesogenetic anhydrite cement is suggested by Purvis (1992) for the Rotliegende sandstones.

The expected isotopic composition for marine-derived Carboniferous anhydrite is around +14‰ $\delta^{34}S_{CDT}$ and 16.6‰ $\delta^{18}O_{V\text{-}SMOW}$ (Claypool et al., 1980) but Juruá anhydrite yielded values between 9.5‰ and 17.8‰ $\delta^{34}S_{CDT}$ (Table 4). Thus, the sulfur isotopic composition of Juruá anhydrite cements deviates significantly from the composition of cements of purely marine origin. Also the two analyzed interbedded evaporitic layers (Table 4) show isotopic values that deviate from purely marine values, probably indicating a fractionation process. This suggests that, although the mesogenetic anhydrite cements may have derived from the dissolution of the interbedded sulfate beds during burial, another mechanism must be considered to explain the abnormal $\delta^{34}S_{CDT}$ values. The most likely would involve the depletion in ^{34}S of the pore fluids due to the precipitation of early diagenetic sulfate nodules (Strauss, 1997). One of the samples in Fig. 7 shows a concomitant depletion of ^{34}S and enrichment in ^{18}O. Such values could correspond to dissolved sulfate modified by progressive evaporation in a *playa lake*, such as modeled by Raab and Spiro (1991) and applied by Amthor and Okkerman (1998) to Rotliegende anhydrite cements.

Table 4
Sulphur and Oxigen isotopes in anhydrites from the Juruá Formation

Well	Depth (m)	Sub-unit	$\delta^{34}S$ (CDT)	$\delta^{18}O$ (V-SMOW)	$\delta^{18}O$ (V-PDB)
RUC-5[a]	2535.4	JR-80	17.7	12.6	(−17.7)
LUC-3[a]	2450	JR-90A	17	11.8	(−18.5)
RUC-1	2442.9	JR-70A	12.9		
RUC-1	2548.6	JR-90B	10.4		
RUC-5	2508.3	JR-70B	16.6	12.2	(−18.1)
RUC-5	2512.5	JR-70B	14.8		
RUC-5	2550.9	JR-90A	16		
RUC-7	2494.8	JR-70B	16.5	12.3	(−18)
RUC-7	2507.1	JR-85	16.3	12.2	(−18.1)
RUC-10	2499.8	JR-70A	17	12.1	(−18.2)
RUC-10	2514	JR-70B	17.8	11.1	(−19.2)
RUC-10	2522.7	JR-70B	16.8	11.9	(−18.4)
RUC-12	2485	JR-70A	11.5		
RUC-12	2498.8	JR-70B	16.7		
RUC-12	2527.8	JR-85	14.9		
RUC-36	2515	JR-70B	13.2	13	(−17.3)
RUC-36	2521.4	JR-70B	17.5		
LUC-1	2439.2	JR-80	16.7	12.5	(−17.8)
LUC-1	2448.2	JR-90A	12.6	12.7	(−17.6)
LUC-3	2447.7	JR-90A	14.2	10.5	(−19.7)
LUC-27	2464.6	JR-70A	9.5	15.4	(−14.9)
LUC-27	2478.4	JR-70B	16.6	11	(−19.3)
IMT-3	2464.3	JR-70B	15.9	11	
IMT-3	2485.5	JR-80	10.7	10.8	(−19.4)

[a] Evaporites.

Further evidence on the origin of the Juruá anhydrite cements is supplied by their strontium isotopic composition, which ranges from 0.7096907 to 0.7137169 (Table 2). These radiogenic values also strongly deviate from Carboniferous sea water composition (Fig. 6), and suggest extensive water–rock interaction and silicate dissolution during burial. The strontium isotopic ratio of the interbedded evaporite layer ($^{87}Sr/^{86}Sr$=0.7089167) also deviates from marine Carboniferous values towards radiogenic input, suggesting recrystallization during burial under influence of diagenetically modified fluids.

The oxygen isotopic composition of the analyzed samples from Juruá anhydrite cements shows very low values (Table 4;

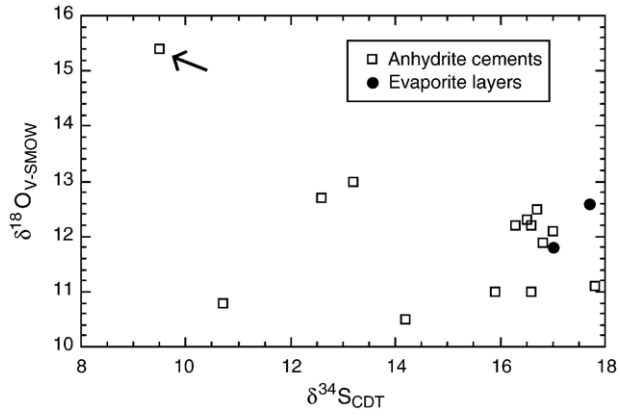

Fig. 7. Diagram of the $\delta^{18}O_{V\text{-}SMOW}$ and $\delta^{34}S_{CDT}$ values of anhydrite cements from Juruá reservoirs. The arrow indicates the possible playa lake evaporation.

Fig. 7). Calculations of the probable precipitation temperatures of the anhydrite cements using Chiba et al. (1981) equation and the same +3‰ value of $\delta^{18}O_{water}$ used to calculate the temperature of the mesodiagenetic dolomite cements (Table 1) would yield unrealistically high temperatures of 161–240 °C. Therefore, these isotopic compositions cannot be explained by thermal re-equilibration with diagenetically evolved pore fluids as the results would be more enriched in ^{18}O. Chiba et al. (1981) consider that anhydrites are in isotopic disequilibrium with the fluids at low temperatures, reaching isotopic equilibrium only at temperatures higher than 200 °C. Similar anomalously low $\delta^{18}O$ values found in anhydrites of the Mississippi Basin are explained by Dworkin and Land (1994) as derived from the oxidation of dissolved sulfide. A similar oxidation of sulfide to sulfate during burial could account for the light isotopic oxygen values found in Juruá anhydrites (Mizutani and Rafter, 1969; Dworkin and Land, 1994). Such oxidation of dissolved sulfide may be related to the voluminous Triassic (200 Ma) igneous activity expressed by large diabase intrusions in the Juruá area (Mizusaki et al., 2002). Fluids of high oxygen fugacity and/or rich in reactive metals may have circulated in association with the enhanced thermal flow related to the Triassic magmatism, causing the oxidation of aqueous sulfide (Mizutani and Rafter, 1969). The Triassic magmatism is also possibly related to the authigenesis of illite in the sandstones, as discussed previously.

7.4. Illite dating, magmatism and tectonism

The ^{40}K–^{40}Ar dating of the authigenic illites revealed two main times of precipitation (Table 3). The ages around 200 Ma are related to the voluminous basic magmatism represented by large diabase sills intruded in the Paleozoic section in the area (Mizusaki et al., 2002). This magmatism has also been related to the generation, expulsion, migration and accumulation of hydrocarbons in the basin (Figueiredo and Milani, 2000). The authigenesis of illite would be related to the enhanced thermal and fluid flow connected to the magmatism, and not to the direct thermal effect of the intrusions. The sampling points for illite dating were selected in order to avoid a possible direct thermal effect of the intrusions. A similar pattern of episodic illite authigenesis has been interpreted for sections of the North Sea by Gluyas et al. (1993). The ages around 150 Ma are interpreted as connected to the compressive tectonism which affected the area (Caputo and Silva, 1990). This tectonism, expressed by large reverse and transpressional structures, would have induced large-scale fluid flow and fracturing of the evaporite and shale seals interbedded to the reservoirs, communicating sandstone bodies that were isolated since first oil migration (Mizusaki et al., 1990). Illites from reservoirs JR-60, JR-70B and JR-90B in RUC field were dated around 200 Ma, which would correspond to the first generation of illites associated to the magmatism and hydrocarbon emplacement. The age around

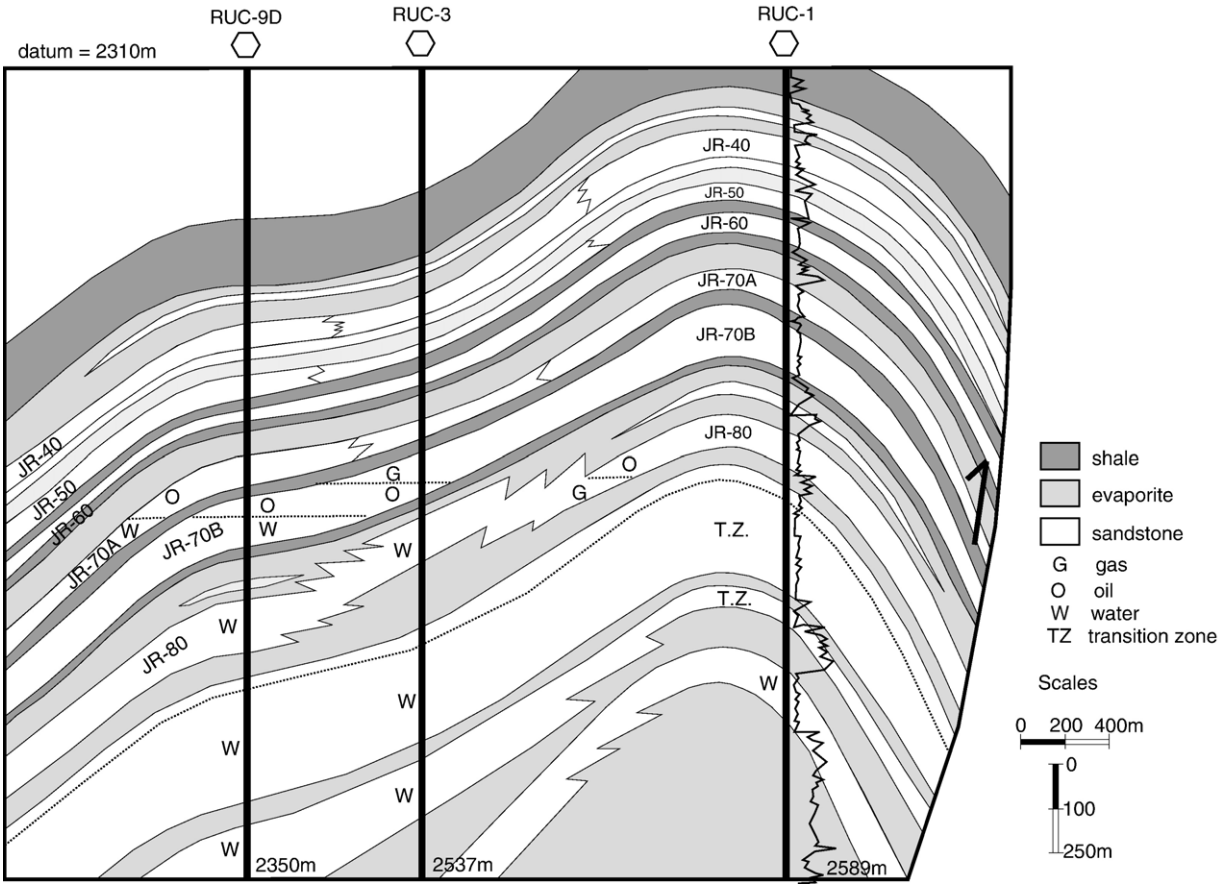

Fig. 8. Schematic structural section across part of RUC field showing major reservoir units (modified from Mizusaki et al., 1990).

150 Ma obtained from reservoir JR-70A was associated to the tectonic rupture of the anhydrite seals which kept this reservoir isolated before the Jurassic–Cretaceous tectonism (Fig. 8).

7.5. Diagenetic evolution of the sandstones

The diagenetic evolution of the Juruá sandstones was defined based on the textural relationships among the diagenetic minerals, on their relative timing with compaction, and on their isotopic and elemental composition.

The diagenetic sequence of eolian and non-eolian sandstones shows differences in the incidence and intensity of some diagenetic processes (Fig. 9), but a nearly general evolution trend can be recognized for all sandstones, comprising (1) eodiagenesis, characterized by coatings of hematite, coatings of mechanically infiltrated clays, framboidal pyrite, microcrystalline and blocky dolomite, and mechanical compaction; (2) mesodiagenesis, characterized by chemical compaction, quartz and K-feldspar overgrowths, feldspar dissolution and albitization, poikilotopic anhydrite, fibrous illite and Fe-dolomite/ankerite, in places by chlorite, calcite and siderite; (3) locally exposure to meteoric influx and telodiagenesis, characterized by hematite and kaolinite, followed by renewed burial and mesodiagenesis.

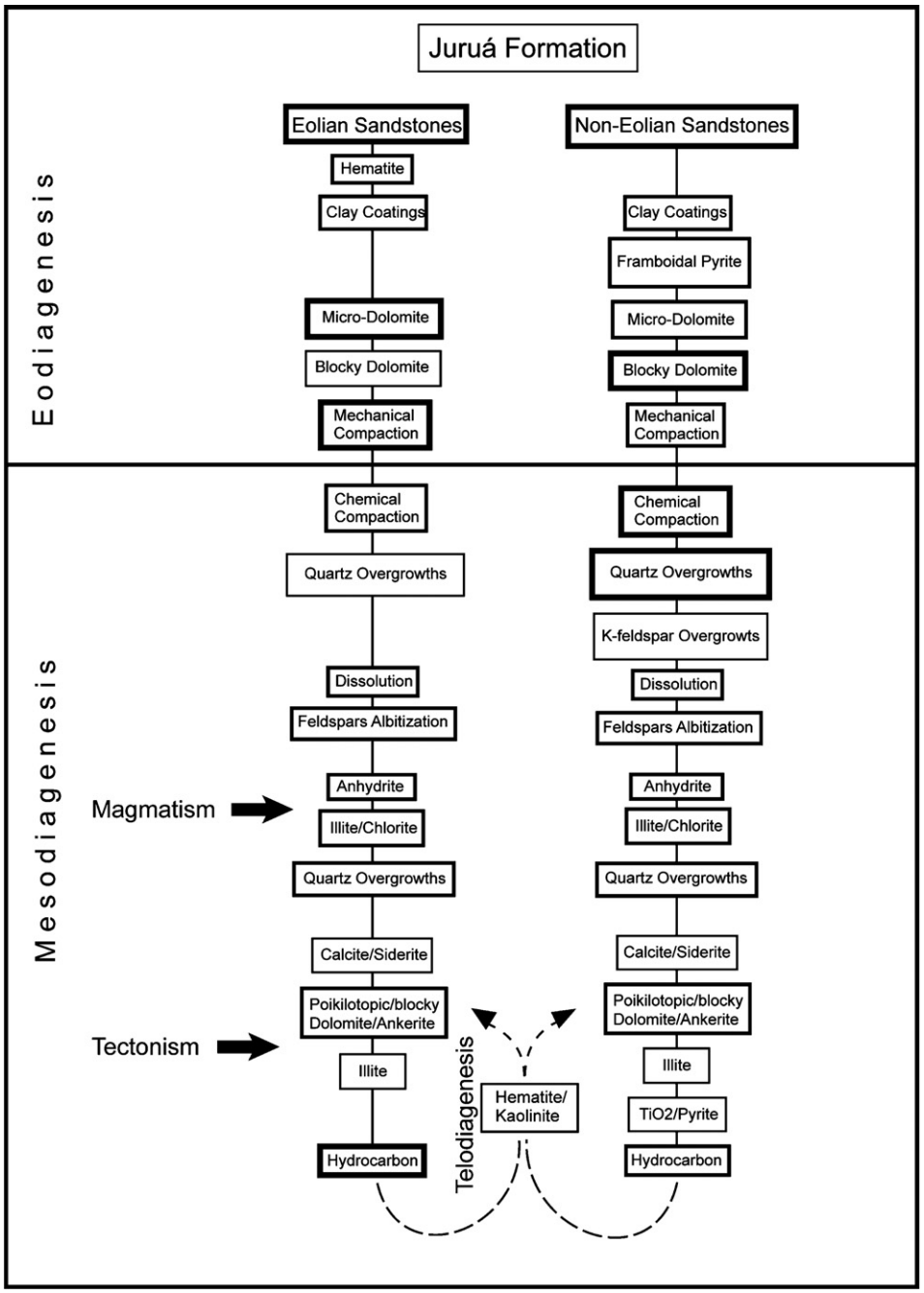

Fig. 9. Main diagenetic evolution pathways in Juruá eolian and non-eolian sandstones (modified from Elias et al., 2004). Discussion in the text.

Integrated diagenetic histories can be interpreted for the western area (RUC field) and the eastern area (LUC and IMT fields) (Figs. 10 and 11), based on the paragenetic relationships recognized in the petrography and the isotopic results. In these diagrams, the importance of the eodiagenetic processes in the evolution of the Juruá sandstones is evident. Most of these early diagenetic processes are related to the availability of concentrated surface fluids related to strong evaporation in the coastal sabkha environment. Other striking feature of these diagenetic histories is the influence of the late Triassic magmatism (200 Ma) and of the Jurassic tectonism (150 Ma) on the mesodiagenetic processes, mostly on the authigenesis of illite, anhydrite, late dolomite/ankerite cements and the albitization of feldspars. The telodiagenetic processes of hematite and kaolinite authigenesis are very light in the studied areas, which are away from the margins of the basin, where they were more intense.

8. Conclusions

The isotopic study of some of the main diagenetic constituents of the Juruá reservoirs of the Urucu area from the Solimões Basin revealed the major conditions and episodes of the diagenetic processes which strongly affected the reservoirs. Such understanding is essential for the development of geochemical models in order to predict the quality of the Juruá reservoirs in the basin and to optimize hydrocarbon production from the analyzed fields.

The Juruá sandstones are mostly subarkoses and arkoses, cemented by dolomite, anhydrite and/or quartz, with minor illite, siderite, pyrite, albite, K-feldspar, chlorite and titanium minerals. Dolomite and anhydrite cementation, together with compaction, exerts the main control on the quality of the reservoirs. The diagenetic sequence of the sandstones comprises eodiagenetic coatings of hematite, coatings of mechanically infiltrated clays, framboidal pyrite, microcrystalline and blocky dolomite, mechanical and chemical compaction, mesodiagenetic quartz and K-feldspar overgrowths, poikilotopic anhydrite, feldspar dissolution and albitization, fibrous illite and Fe-dolomite/ankerite, in places, chlorite, calcite and siderite. Locally, exposure to telodiagenetic meteoric influx generated hematite and kaolinite, followed by new burial and mesodiagenesis.

Dolomite occurs as eogenetic microcrystalline rim and pore-fill cements, as grain-displacive blocky cement, and as mesodiagenetic grain-replacive poikilotopic and blocky cements. The $\delta^{18}O_{V\text{-}PDB}$ values of the eodiagenetic dolomite

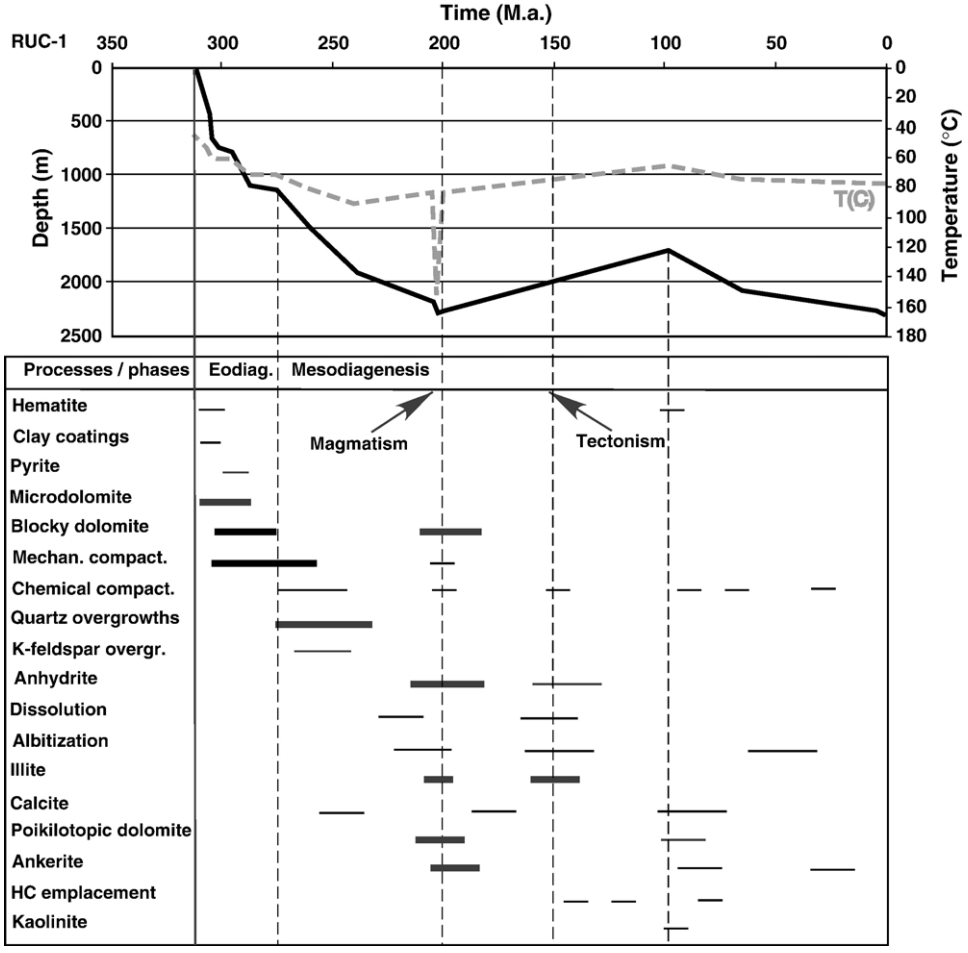

Fig. 10. Burial, thermal and diagenetic history of the reservoirs from the western studied area (RUC field—burial history curve was constructed using backstripping and Petrobras informations).

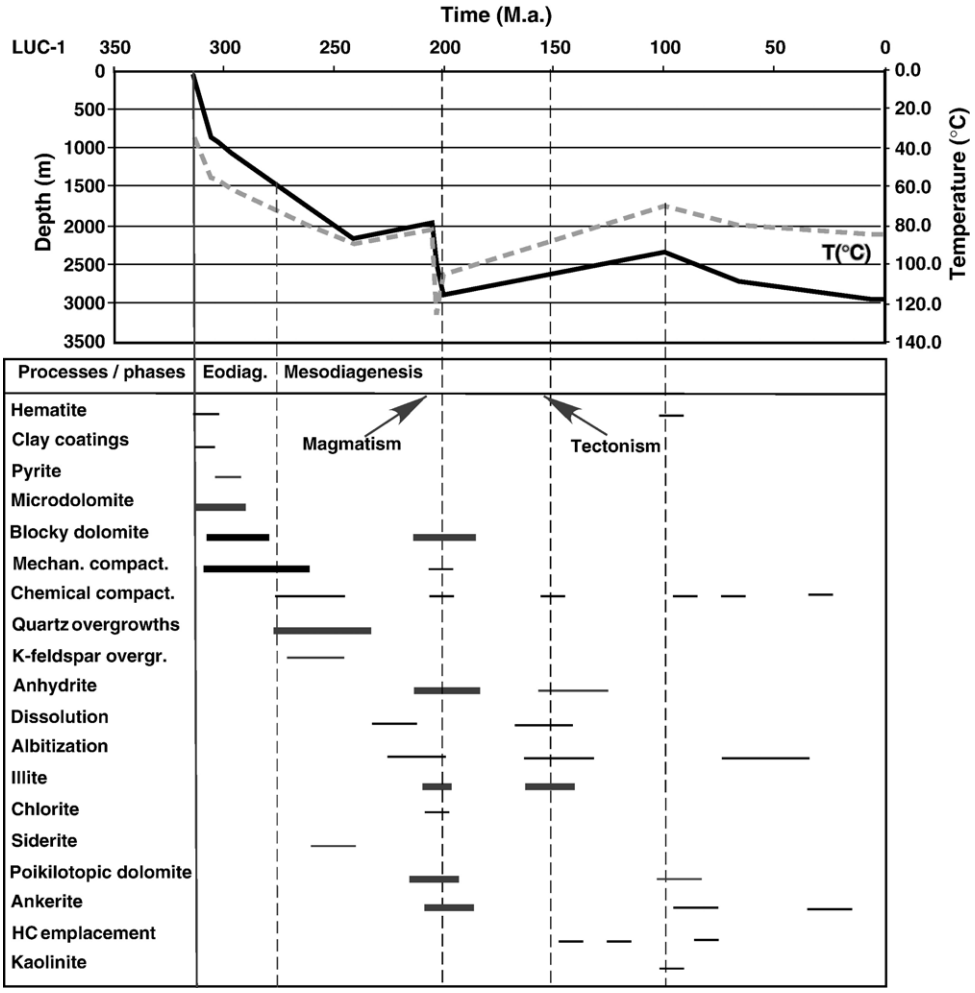

Fig. 11. Burial, thermal and diagenetic history of the reservoir from the eastern studied area (LUC field—burial history curve was constructed using backstripping and Petrobras information).

cements indicate precipitation temperatures of 34–70 °C and their $\delta^{13}C_{V\text{-}PDB}$ values suggest an initial marine carbonate source modified by meteoric inflow and bacterial sulfate reduction. The dominant occurrence of microcrystalline dolomite in eolian sandstones suggests precipitation from pore fluids highly concentrated due to evaporation. Interaction between inflowing meteoric waters and silicates is also suggested by the $^{87}Sr/^{86}Sr$ ratio values between 0.7097048 and 0.7123545, which deviate from Carboniferous marine values.

The $\delta^{18}O_{V\text{-}PDB}$ values of the mesodiagenetic poikilotopic and blocky dolomite cements can be associated with precipitation at temperatures of 99–155 °C, assuming a $\delta^{18}O_{water}$ value of +3‰. The $\delta^{13}C_{V\text{-}PDB}$ values of these dolomites, in a positive trend with the oxygen, suggest the gradual input from thermal decarboxylation of organic mater over the initial marine source. The $^{87}Sr/^{86}Sr$ ratio values between 0.7146637 and 0.7219222 indicate a very extensive water–rock interaction, with input of radiogenic ^{87}Sr from silicate dissolution. Minor calcite and siderite cements are within the general isotopic trend of burial dolomite cements.

Anhydrite cements are more abundant in sandstones with less dolomite, occurring as pore-filling, poikilotopic cement heterogeneously distributed as scattered spots, or selectively cementing the coarser laminations. Anhydrite covers quartz overgrowths and engulfs microcrystalline and blocky dolomite. The $\delta^{34}S_{CDT}$ values of anhydrite cements from 9.5‰ to 17.8‰ deviates from purely marine cements, suggesting derivation from the burial dissolution of interbedded nodular sulfates, and/or from the depletion in ^{34}S of the pore fluids due to the precipitation of eodiagenetic sulfate nodules. Anhydrite $\delta^{18}O_{V\text{-}PDB}$ values as low as −19.75‰ are in clear disequilibrium with the fluids, being possibly connected to the oxidation of dissolved sulfide, may be related to the voluminous Triassic basic magmatism. Intense fluid–rock interaction during anhydrite precipitation is also indicated by the very radiogenic $^{87}Sr/^{86}Sr$ ratios from 0.7096907 to 0.7137169.

Most of the eodiagenetic processes are related to the availability of concentrated surface fluids related to strong evaporation in the coastal sabkha environment. The late Triassic magmatism (200 Ma) and of the Jurassic tectonism (150 Ma) exerted strong influence on the mesodiagenetic processes, mostly on the authigenesis of illite, as suggested by its K–Ar ages, on the late anhydrite and dolomite/ankerite cementation and on the albitization of feldspars.

Acknowledgements

The authors thank Petrobras for access to samples, data, information, and for the license to publish this work. Special acknowledgements to the research support granted by Brazil National Research Council-CNPq. We acknowledge the access to the support and analytical facilities of the Institute of Geosciences of Rio Grande do Sul Federal University.

References

Al-Aasm, I.S., Taylor, B.E., South, B., 1990. Stable isotope analysis of multiple carbonate samples using selective acid extraction. Chemical Geology 80, 119–125.

Amaral, G., Cordani, U.G., Kawashita, K., Reynolds, J.H., 1966. Potassium-Argon dates of basaltic rocks from southern Brazil. Geochimica et Cosmochimica Acta 30, 150–184.

Amthor, J.E., Okkerman, J., 1998. Influence of early diagenesis on reservoir quality of Rotliegende Sandstones, Northern Netherlands. American Association of Petroleum Geologists Bulletin 82, 2246–2265.

Anjos, S.M.C., De Ros, L.F., Souza, R.S., Silva, C.M.A., Sombra, C.L., 2000. Depositional and diagenetic controls on the reservoir quality of Lower Cretaceous Pendência sandstones, Potiguar rift basin, Brazil. American Association of Petroleum Geologists Bulletin 84, 1719–1742.

ANP (Agência Nacional do Petróleo), 2006. Rio de Janeiro, Brasil, ANP. Available at htpp://www.brazil-rounds.gov.br/round5/Solimões.asp.

Becker, C.R., 1997. Estratigrafia de Sequências Aplicada ao Permo-Carbonífero da Bacia do Solimões do Norte do Brasil. Brazil, Master Thesis, Universidade Federal do Rio Grande do Sul.

Boles, J.R., 1978. Active ankerite cementation in the subsurface Eocene of southwest Texas. Contributions to Mineralogy and Petrology 68, 13–22.

Burke, W.H., Denison, R.E., Hetherington, E.A., Koepnick, R.B., Nelson, H.F., Oto, J.B., 1982. Variation of seawater $^{87}Sr/^{86}Sr$ throughout Phanerozoic time. Geology 10, 516–519.

Camoleze, Z., Silva, E.S.O., Kinzel, J.M., Corrêa, J.R.B., 1990. Província do Rio Urucu- Seqüências Sedimentares e Fácies Reservatório-Bacia do Solimões. Seminário de Geologia de Desenvolvimento e Reservatório 4 (1), 1–11.

Caputo, M.V., Silva, O.B., 1990. Sedimentação e tectônica da Bacia do Solimões. In: Raja Gabaglia, G.P., Milani, E.J. (Eds.), Origem e Evolução das Bacias Sedimentares, Petrobras, pp. 169–193.

Carothers, W.W., Adami, L.H., Rosenbauer, R.J., 1988. Experimental oxygen isotope fractionation between siderite-water and phosphoric acid-liberated CO_2-siderite. Geochimica et Cosmochimica Acta 52, 2445–2450.

Chiba, H., Kusakabe, M., Hirano, S.I., Matsuo, S., Somiya, S., 1981. Oxygen isotope fractionation factors between anhydrite and water from 100 to 550 °C. Earth and Planetary Science Letters 53, 55–62.

Claypool, G.E., Holser, W.T., Kaplan, I.R., Sakai, H., Zak, I., 1980. The age curves of sulfur and oxygen in marine sulfate and their mutual interpretation. Chemical Geology 28, 199–260.

Craig, H., 1957. Isotopic standards for carbon and oxygen correction factors for mass spectrometric analysis of carbon dioxide. Geochimica et Cosmochimica Acta 12, 133–149.

Cunha, P.R.C., Silva, O.B., Eiras, J.F., 1988. Interpretação faciológica e ambiental do principal reservatório de hidrocarbonetos da Bacia do Solimões-Área do Urucu. Congresso Brasileiro de Geologia 35 (1), 2439–2456.

Dixon, S.A., Summers, D.M., Surdam, R.C., 1989. Diagenesis and preservation of porosity in Norphlet formation (Upper Jurassic), southern Alabama. American Association of Petroleum Geologists Bulletin 73, 707–728.

Dworkin, S.I., Land, L.S., 1994. Petrographic and geochemical constraints on the formation and diagenesis of anhydrite cements, Smackover sandstones, Gulf of Mexico. Journal of Sedimentary Research A64, 339–348.

Eiras, J.F., Becker, C.R., Souza, E.M., Gonzaga, F.G., Silva, J.G.F., Daniel, L.M.F., Matsuda, N.S., Feijó, F.J., 1994. Bacia do Solimões. Boletim de Geociências da Petrobras 8, 17–45.

Elias, A.R.D., De Ros, L.F., Mizusaki, A.M.P., Anjos, S.M.C., 2004. Diagenetic patterns in eolian/coastal sabkha reservoirs of the Solimões Basin, northern Brazil. Sedimentary Geology 169, 191–217.

Figueiredo, A.M., Milani, E.J., 2000. Petroleum systems of South America basins. In: Cordani, U.G., Milani, E.J., Tomaz Filho, A., Campos, D.A. (Eds.), Tectonic Evolution of South America: Rio de Janeiro, pp. 689–718.

Fisher, R.S., Land, L.S., 1986. Diagenetic history of Eocene Wilcox sandstones, South-Central Texas. Geochimica et Cosmochimica Acta 50, 551–561.

Folk, R.L., 1968. Petrology of Sedimentary Rocks. Hemphill, Texas. 107 pp.

Gauthier, D.L., 1982. Siderite concretions: indicator of early diagenesis in the Gammon Shale (Cretaceous). Journal of Sedimentary Petrology 52, 859–871.

Gluyas, J.G., Grant, S.M., Robinson, A.G., 1993. Geochemical evidence for a temporal control on sandstone cementation. In: Horbury, A., Robinson, A. (Eds.), Diagenesis and Basin Development. Studies in Geology, vol. 36. American Association of Petroleum Geologists, pp. 23–33.

Hendry, J.P., Wilkinson, M., Fallick, A.E., Haszeldine, R.S., 2000. Ankerite cementation in deeply buried Jurassic sandstones reservoirs of the Central North Sea. Journal of Sedimentary Research 70, 227–239.

James, W.C., 1992. Sandstone diagenesis in mixed siliciclastic-carbonate sequences: Quadrant and Tensleep formations (Pennsylvanian), northern Rocky Mountains. Journal of Sedimentary Petrology 62, 810–824.

Land, L.S., Fisher, R.S., 1987. Wilcox sandstone diagenesis, Texas Gulf Coast: a regional isotopic comparison with the Frio Formation. In: Marshall, J.D. (Ed.), Diagenesis of Sedimentary Sequences. Geological Society Special Publication, pp. 219–235.

Lanzarini, W.L., 1984. Fácies Sedimentares e Ambiente Deposicional da Formação Monte Alegre na área do Juruá, Bacia do Alto Amazonas- Diagênese e Permoporosidade dos Arenitos Reservatórios. Brazil, Master Thesis, Universidade Federal de Ouro Preto.

Macaulay, C.I., Fallick, A.E., McLaughlin, O.M., Haszeldine, R.S., Pearson, M.J., 1998. The significance of $\delta^{13}C$ of carbonate cements in reservoir sandstones: a regional perspective from the Jurassic of the northern North Sea. In: Morad, S. (Ed.), Carbonate Cementation in Sandstones. International Association of Sedimentologists. Blackwell Scientific Publications, pp. 395–408.

Mankiewicz, D., Steidtmann, J.R., 1979. Depositional environments and diagenesis of the Tensleep Sandstone, Eastern Big Horn Basin, Wyoming. In: Scholle, P.A., Schluger, P.R. (Eds.), Aspects of Diagenesis. SEPM Special Publication. Society of Economic Paleontologists and Mineralogists, pp. 319–336.

Milani, E.J., Zalán, P.V., 1998. Solimões Basin, The Geology of Paleozoic Cratonic Basins and Mesozoic Interior Rifts of Brazil. The American Association of Petroleum Geologists, Special Publication 67–90.

Mizutani, Y., Rafter, T.A., 1969. Oxygen isotopic compositions of sulfates: 3. Oxygen isotopic fractionation in the bisulfate ion-water system: New Zealand. Journal of Science 12, 54–59.

Mizusaki, A.M.P., Anjos, S.M.C., Wanderley, J.W., Silva, O.B., Costa, M.G.F., Lima, M.P., Kawashita, K., 1990. Datação K/Ar de ilitas diagenéticas. Boletim de Geociências da Petrobras 4, 237–252.

Mizusaki, A.M.P., Thomaz-Filho, A., Milani, E.J., Césero, P., 2002. Mesozoic and Cenozoic igneous activity and its tectonic control in northeastern Brazil. Journal of South America Earth Sciences 15, 183–198.

Morad, S., Marfil, R., Al-Aasm, I.S., Gomez-Gras, D., 1992. The role of mixing-zone dolomitization in sandstone cementation: evidence from the Triassic Buntsandstein, the Iberian Range, Spain. Sedimentary Geology 80, 53–65.

Morad, S., Al-Aasm, I.S., Longstaffe, F.J., Marfil, R., De Ros, L.F., Johansen, H., Marzo, M., 1995. Diagenesis of a mixed siliciclastic/evaporitic sequence of the Middle Muschelkalk (Middle Triassic), the Catalan Coastal Range, NE Spain. Sedimentology 42, 749–768.

Morad, S., Worden, R.H., Ketzer, J.M., 2003. Oxygen and hydrogen isotopic composition of diagenetic clay minerals in sandstones: a review of the data and controls. In: Worden, R.H., Morad, S. (Eds.), Clay Mineral Cements in Sandstones. International Association of Sedimentologists. Blackwell Scientific Publications, pp. 63–92.

Moraes, M.A.S., De Ros, L.F., 1990. Infiltrated clays in fluvial Jurassic sandstones of Recôncavo Basin, northeastern Brazil. Journal of Sedimentary Petrology 60, 809–819.

Moraes, M.A.S., De Ros, L.F., 1992. Depositional, infiltrated and authigenic clays in fluvial sandstones of the Jurassic Sergi Formation, Recôncavo Basin, northeastern Brazil. In: Houseknecht, D.W., Pittman, E.W. (Eds.), Origin, Diagenesis and Petrophysics of Clay Minerals in Sandstones. Society of Economic Paleontologists and Mineralogists, pp. 197–208.

Neto, A.F.A., Tsubone, K., 1988. A descoberta de petróleo do Rio Urucu, Bacia do Solimões. Congresso Brasileiro de Geologia 35, 2416–2426.

Platt, J.D., 1994. Geochemical evolution of pore waters in the Rotliegend (Early Permian) of northern Germany. Marine and Petroleum Geology 11, 66–78.

Purvis, K., 1992. Lower Permian Rotliegend sandstones, southern North Sea: a case study of sandstone diagenesis in evaporite-associated sequences. Sedimentary Geology 77, 155–171.

Pye, K., Krinsley, D.H., 1986. Diagenetic carbonate and evaporite minerals in Rotliegend aeolian sandstones of the southern North Sea: their nature and relationship to secondary porosity development. Clay Minerals 21, 443–457.

Raab, M., Spiro, B., 1991. Sulfur isotopic variations during seawater evaporation with fractional crystallization. Chemical Geology 86, 323–333.

Rosenbaum, J.M., Sheppard, S.M.F., 1986. An isotopic study of siderites, dolomites and ankerites at high temperatures. Geochimica et Cosmochimica Acta 50, 1147–1150.

Schmidt, V., McDonald, D.A., 1979. The role of secondary porosity in the course of sandstone diagenesis. In: Scholle, P.A., Schluger, P.R. (Eds.), Aspects of Diagenesis. Society of Economic Paleontologists and Mineralogists, pp. 175–207.

Schultz, J.L., Boles, J.R., Tilton, G.R., 1989. Tracking calcium in the San Joaquin basin, California: a strontium isotopic study of carbonate cements at North Coles Levee. Geochimica et Cosmochimica Acta 53, 1991–1999.

Souza, R.S., De Ros, L.F., Morad, S., 1995. Dolomite diagenesis and porosity preservation in lithic reservoirs: Carmópolis Member, Sergipe-Alagoas Basin, northeastern Brazil. American Association of Petroleum Geologists Bulletin 79, 725–748.

Steiger, R.H., Jager, E., 1977. Subcomission on Geochronology convention on the use of decay constants in geochronology and cosmochronology. Earth and Planetary Science Letters 36, 359–362.

Strauss, H., 1997. The isotopic composition of sedimentary sulfur through time. Palaeogeography, Palaeoclimatology, Palaeoecology 132, 97–118.

Sullivan, M.D., Haszeldine, R.S., Fallick, A.E., 1990. Linear coupling of carbon and strontium isotopes in Rotliegend Sandstone, North Sea: evidence for cross-formational fluid flow. Geology 18, 1215–1218.

Thode, H.G., Monster, J., Dunford, H.B., 1961. Sulphur isotope geochemistry. Geochimica et Cosmochimica Acta 25, 150–174.

Veizer, J., 1992. Depositional and diagenetic history of limestones: stable and radiogenic isotopes. In: Clauer, N., Chaudhuri, S. (Eds.), Isotopic Signatures and Sedimentary Records. Springer-Verlag, pp. 13–48.